Stable Superhydrophobic Organic−Inorganic Hybrid Films by Electrostatic Self-Assembly

Joong Tark Han, Yanli Zheng, Jeong Ho Cho, Xurong Xu, and Kilwon Cho*

Department of Chemical Engineering, Polymer Research Institute, Pohang University of Science and Technology, Pohang, 790-784, Korea

Received: May 23, 2005; In Final Form: September 11, 2005

Organic−inorganic hybrid films were prepared through layer-by-layer (LBL) deposition of poly(allylamine hydrochloride) (PAH) and ZrO_2 nanoparticles coated with poly(acrylic acid) (PAA), allowing facile control of surface roughness and hydrophobicity. Superhydrophobic behavior was observed after deposition of silica nanoparticles and a simple fluorination of the surface. The structure of films was controlled by the number of deposition cycles using PAA-coated 100 nm ZrO_2 nanoparticles, the particle size, and the prelayer with PAH and PAA. The change in the apparent water contact angle of $(PAH/PAA\text{-coated } ZrO_2)_n$ surfaces without fluorination of the surface agrees with Cassie and Baxter's model for nonwetted surfaces even though the outermost surface itself is hydrophilic. Superhydrophobic surfaces were then successfully developed by the deposition of hydrophilic silica nanoparticles on a 10 bilayer surface of PAH/PAA-coated ZrO_2, and a simple fluorination. Moreover, the chemical stability of the film was greatly increased by heat-induced cross-linking of the film. The incorporation of ZrO_2 nanoparticles in superhydrophobic films promises better mechanical properties than the organic film.

Introduction

The layer-by-layer (LBL) processing of polyelectrolyte multilayers can be used to coat complex substrates,[1] and has shown promise in various applications such as in sensors, electronics, functional films, bioadhesives, membranes, hollow capsules, and hard coatings.[2−9] Previously, we constructed a stable organic−inorganic hybrid multilayer film by coating ZrO_2 nanoparticles with poly(4-sodium styrenesulfonate) (PSS), combining those with a diazo resin, and irradiating the resulting multilayer film with UV.[10] This type of organic−inorganic nanocomposite film is a leading candidate for protective coatings with greater toughness and strength than simple ceramic or polymeric coatings. Since these new nanocomposite films can have higher stability, greater hardness, and increased surface functionality, research on polyelectrolyte/ZrO_2 nanoparticle films may create far-reaching insights and lead to more important applications for these materials.

Furthermore, the wettability control of a solid surface has recently attracted much attention from material scientists. This is governed by both the chemical composition and the geometric microstructure of the surface; the wettability can be decreased by creating a local geometry with a large geometric area relative to the projected area. This effect can be observed in nature on the leaves of the sacred lotus.[11−17] Surfaces with contact angles for water of greater than 150° have attracted much attention because of their potential practical applications as self-cleaning surfaces and as low flow resistance coatings in microfluidic systems.[18−20] Therefore, many methods have been made to fabricate artificial superhydrophobic surfaces, such as LBL processing,[21−24] sol−gel process,[25−27] generation of fibrillar structure on surfaces,[28−31] creation of a rough surface covered with low surface energy molecules,[32−37] phase separation of a polymer in a mixed solvent system,[38] and others.[39−41]

Recently, Shiratori and co-workers[21] have reported ultra-water-repellent surfaces having a complicated microstructure of SiO_2 nanoparticles by using the electrostatic self-assembly process, in which films were treated at high temperature 650 °C for 1 h to remove polyelectrolyte, followed by surface hydrophobic treatment. In another report, the use of a polyelectrolyte multilayer as a preformed matrix in electrochemical deposition of gold clusters, leading to the fabrication of a superhydrophobic surface, was reported by Zhang and co-workers.[22] They demonstrated the superhydrophobic surface created by the dendritic gold clusters on an indium tin oxide electrode covered with a polymer multilayer film through electrochemical deposition. Since then, a method of generating ultrahydrophobic surfaces from a combination of fluorinated polyelectrolyte and clay has been reported by Schlenoff and co-workers.[23] These recent methods used to create a superhydrophobic surface, however, limit the application because of the high process temperature, the specific deposition condition, and the low chemical/mechanical durability.

In addition, related to our present study, Rubner and co-workers[24] have reported superhydrophobic surfaces by use of microporous polyelectrolyte multilayers, silica nanoparticles, and a hydrophobic surface treatment. Although they have described a general method of how to make a superhydrophobic surface via LBL process, their method requires deposition of 100.5 bilayers of oppositely charged polyelectrolytes followed by immersion of this film into a combined acidic solution (pH ≈ 2.7, 2.3) for the formation of micropores. Such a process is not simple, and it would take a long time to fabricate the superhydrophobic coating. Moreover, the organic multilayer film does not promise mechanical durability.

Therefore, we now present a very simple process for the fabrication of a superhydrophobic organic−inorganic nanocomposite coating that requires only over 10 deposition cycles of PAH and PAA-coated ZrO_2 nanoparticles, 1.5 bilayer of PAH/silica nanoparticles, and a simple hydrophobic treatment. Notably, the presence of ZrO_2 nanoparticles in the organic−inorganic nanocomposite film contributes to a higher hardness, an important mechanical property that enlarges the range of potential applications. Moreover, we have managed to make

* To whom correspondence should be addressed. Telephone: +82-54-279-2270. Fax: +82-54-279-8269. E-mail: kwcho@postech.ac.kr.

10.1021/jp052691x CCC: $30.25
Published on Web 10/14/2005

the film stable by inducing cross-linking between PAA and PAH by heating the film.[42]

Experimental Section

Materials. Poly(allylamine hydrochloride) (PAH, molecular weight 70 000), poly(acrylic acid) (PAA, molecular weight 240 000), and nanosilica particles (size ca. 11 nm) were obtained from Aldrich. Two kinds of ZrO_2 nanoparticle colloidal dispersions were obtained from Alfa Aesar with average particle sizes of ca. 5 and 100 nm. 1*H*,1*H*,2*H*,2*H*-Perfluorodecyltrichlorosilane was purchased from Lancaster. The etching mixture was composed of NaCl, H_2O, and DMF organic solvent. All water was Millipore Milli-Q grade with a resistivity of about 18 MΩ/cm and obtained from a Milli-Q purification system (Millipore, USA). All chemicals were used directly without further purification.

Surface Modification of Nanoparticles. PAA-coated ZrO_2 colloid solutions were prepared by the reference method[43] as follows. First, 0.5 mL of ZrO_2 colloid dispersion (20 wt %) was dropped into a PAA solution with a concentration of 0.07mol L^{-1} (with respect to monomer units). This concentration was high enough to ensure excess PAA in order to get more complete adsorption on the surface of the ZrO_2 nanoparticles. The PAA was allowed to adsorb for 20 min with periodic stirring. After sonication for 10 min., the dispersion was then centrifuged for 30 min at 8000 rpm, followed by replacement of the supernatant solution with ultrapure water. The preliminary PAA-coated ZrO_2 colloid was redispersed by shaking. To disperse the colloid particles completely, gentle sonication for 10 min was necessary. Then, the dispersion was centrifuged for 30 min at 8000 rpm. To remove excess or nonadsorbed PAA chains in the mixture, this cleaning process (centrifugation/supernatant exchange by water/redispersion) was repeated three more times. Finally, the dispersion was centrifuged for 10 min at 3000 rpm. The resulting supernatant was a stable suspension of PAA-coated ZrO_2 colloid. It is worth noticing that pH has a great effect on the preparation of the colloid dispersion. Usually the pH of PAA is 5.5−6.0.

Preparation of Superhydrophobic Organic−Inorganic Films. Organic−inorganic nanocomposite films having a multilevel structure were easily prepared by the electrostatic self-assembly method under the condition of pH 5.3 for the PAA-coated ZrO_2 deposition and pH 7.0 for the PAH deposition at room temperature. Prior to the first deposition of PAA-coated ZrO_2, five bilayers of PAH and PAA ($(PAH/PAA)_5$) were deposited onto the cleaned Si wafer to prepare the dense first ZrO_2 layer. The $(PAH/PAA)_5$-coated Si wafer was then immersed in 40 mM PAH solution for 5 min and then rinsed three times with ultrapure water for 1 min each time. The substrate was then dipped into PAA-coated ZrO_2 colloid solution for another 5 min and rinsed three times with ultrapure water. Then, 1.5 bilayers of silica nanoparticles/PAH were deposited on the $(PAH/PAA\text{-coated } ZrO_2)_n$ films using a 0.05% nanosilica aqueous solution and pH 7.0 PAH solution. After the deposition process was complete, the $(PAH/PAA\text{-coated } ZrO_2)_n$ films were heated to 215 °C for 2 h to induce amidation between PAH and PAA chains. The hydrophobization of these organic−inorganic films was performed by dipping films in 1*H*,1*H*,2*H*,2*H*-perflurodecyltrichlorosilane/hexane solution for 1 h, and baking at 120 °C for 20 min.

Characterization. A Nanoscope III (Digital Instrument) in tapping mode and a scanning electron microscope (Hitachi 4200) were used to observe the surface morphology of organic−inorganic nanocomposite films. IR absorption spectra of hybrid films before and after the cross-linking reaction were obtained in single reflection mode using a nitrogen-purged Fourier transform infrared spectrometer (Bruker IFS 66 v FT-IR). The hardness of the films was evaluated by the nanoindentation test using a Hysitron TriboScope nanomechanical testing system attached to an Autoprobe CP scanning probe microscope (Park Scientific Instrument), in which a Berkovich diamond tip (three-sided pyramid, good for hardness and modulus measurements of hard and stiff materials) was used as an indenter. In addition, although 10 deposition cycle samples were used for a superhydrophobic surface, 60 deposition cycle samples were used for hardness tests to avoid the influence of the substrate. Hydrophobicity was confirmed by water contact angle measurement with a 2 mm water droplet.

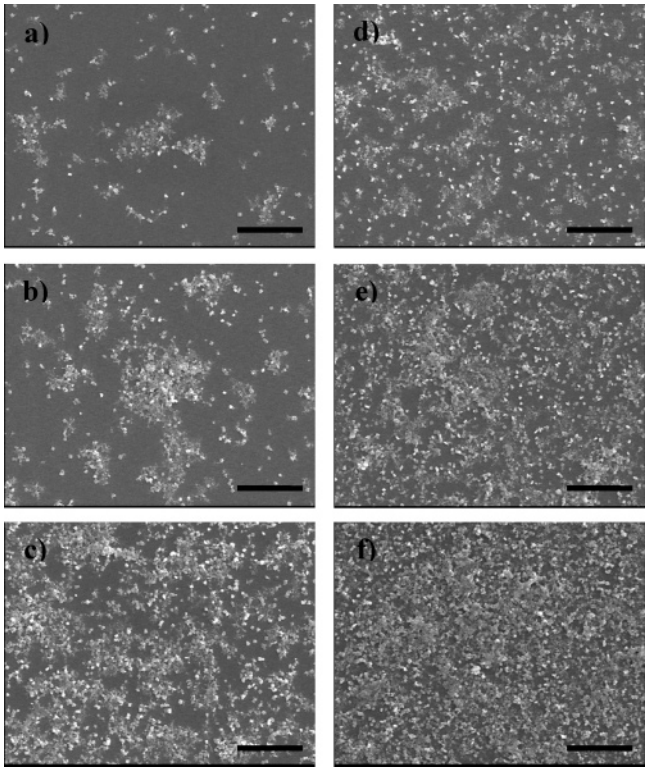

Figure 1. SEM images of organic−inorganic nanocomposite films with PAH/PAA-coated ZrO_2 (100 nm) on Si wafer by sequential deposition cycles: (a−c) without prelayer of $(PAH/PAA)_5$; (d−f) with prelayers of $(PAH/PAA)_5$. (a, d) One deposition cycle; (b, e) two cycles; (c, f) five cycles. Scale bars indicate 3 μm.

Results and Discussion

To fabricate porous organic−inorganic nanocomposite films having a multilevel structure on a negatively charged Si wafer, we used the LBL technique with the commercial polyelectrolytes PAA ($M_w \sim 240\,000$) and PAH ($M_w \sim 70\,000$), in conjunction with ZrO_2 nanoparticles. ZrO_2, one of the leading candidate materials for protective coatings, exhibits promising characteristics such as high strength, fracture toughness, abrasion resistance, and chemical and thermal stability. Figure 1 shows the SEM images of $(PAH/PAA\text{-coated } ZrO_2)_n$ films with $(PAA/PAH)_5$ prelayer (Figure 1a−c) and without prelayer (Figure 1d−f). Obviously, the $(PAH/PAA)_5$ prelayer improves the density of PAA-coated ZrO_2 nanoparticles, which therefore reduces the number of deposition cycles required to attain the desired roughness.

To examine the effect of particle size on surface morphology, we prepared organic−inorganic nanocomposite films using ZrO_2 particles with two different particle diameters, 5 and 100 nm. The 5 nm ZrO_2 particle systems gave flat, well-assembled

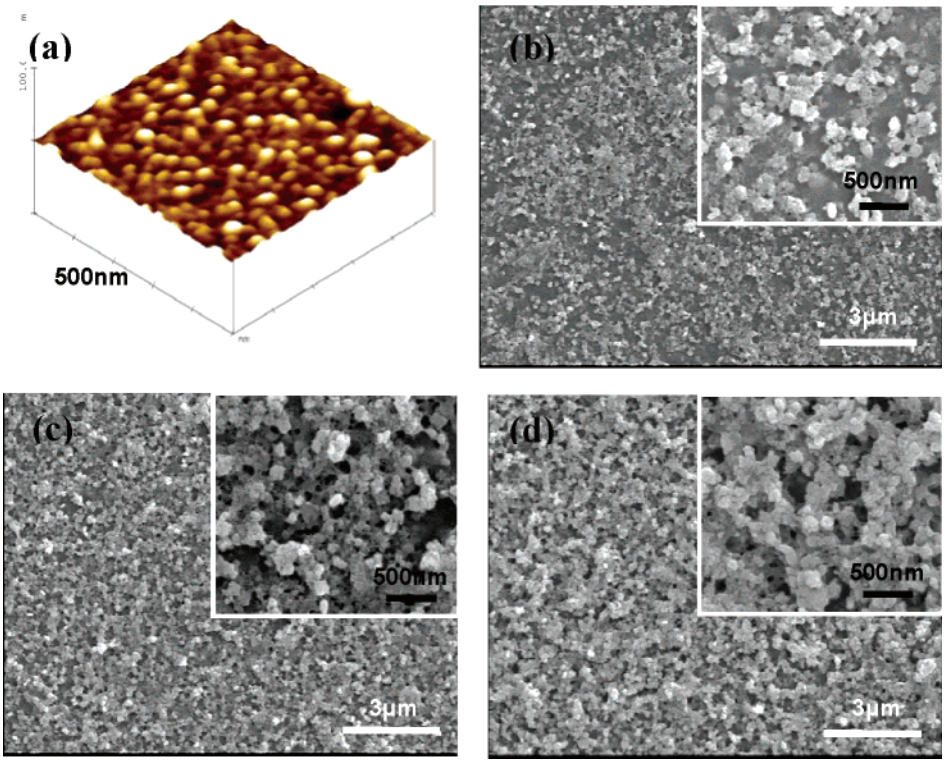

Figure 2. (a) Atomic force microscope image of (PAH/PAA-coated ZrO_2)$_n$ multilayer film with 5 nm ZrO_2 nanoparticles on Si wafer. (b−d) SEM images of organic−inorganic nanocomposite films fabricated by sequential deposition of PAH and PAA-coated ZrO_2 (100 nm) onto Si wafers. The number of deposition cycles for (b), (c), and (d) is 5, 10, and 20, respectively. Insets in (c) and (d) show higher magnification images.

multilayer films (Figure 2a). In these films, the small ZrO_2 nanoparticles may form nanoclusters in the colloid solution, which may lead to very strong intermolecular interactions between clusters in individual layers. However, it is noticeable that scanning electron microscope images of the organic−inorganic nanocomposite films constructed using 100 nm ZrO_2 particles show porous net structures even after over 10 deposition cycles (Figure 2c,d). The morphology of films was controlled by the number of deposition cycles of PAH and PAA-coated ZrO_2 particles; specifically, the surface roughness and porosity after 20 deposition cycles (Figure 2d) was greater than that after five deposition cycles (Figure 2b). Moreover, previously we found that organic−inorganic multilayer films fabricated using strong polyelectrolytes such as poly(styrene sulfonate)-coated ZrO_2 particles and diazo resin were uniform rather than rough, even when 100 nm ZrO_2 nanoparticles were used, in which ZrO_2 nanoparticles may repel each other to produce an even coverage.[10] The homogeneous, dense nanoparticle layer would be formed when there is a good match between the electrostatic attraction of diazo resin and PSS-coated ZrO_2 and the electrostatic repulsion among the PSS-coated ZrO_2 nanoparticles. We therefore speculate that the loose network surface observed in the present work is due to a mismatch of the electrostatic force between weak polyelectrolytes (PAA, PAH) and large nanoparticles (100 nm ZrO_2 nanoparticles).

The water contact angle (CA) increased gradually with increasing number of deposition cycles (Figure 3). After 20 deposition cycles, where a PAH layer was the outermost layer, the advancing and receding water CAs were 139° ± 3°, and 97° ± 3°, respectively, whereas after 10 deposition cycles, the advancing water CA was 110° (Figure 3a). When the outermost layer was PAA-coated ZrO_2, the maximum water CA was about 95°, which was also larger than that of the flat film (48°) (Figure 3b). Compared to the films created by deposition of 100 nm ZrO_2 particles, the organic−inorganic multilayer films prepared

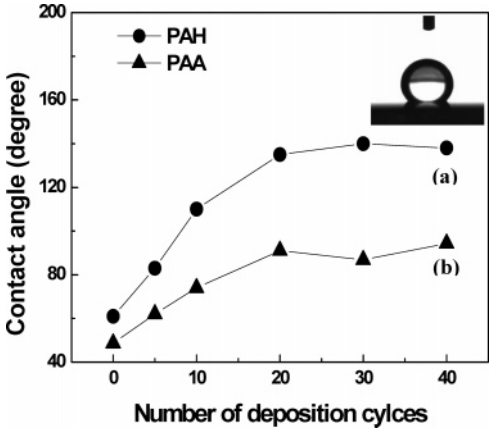

Figure 3. Water contact angle measurements on the surface of organic−inorganic nanocomposite films as a function of number of deposition cycles. Inset is the shape of a water droplet on the surface of (PAH/PAA-coated ZrO_2)$_{20}$ film. The outermost layer is PAH in (a) and PAA in (b).

using PAA-coated 5 nm ZrO_2 particles and PAH gave a maximum water CA of about 90°, indicating that this system is much less promising as a water-repellent coating. Our results agree well with the model of Cassie and Baxter[1b] for nonwetted surfaces. Recently, Abdelsalam et al.[44] have also illustrated that the apparent water contact angle can increase on structured gold surfaces formed by electrodeposition through monolayer templates of close-packed uniform submicrometer spheres even though the gold itself is hydrophilic (water CA = 70°). Furthermore, the hydrophilicity decrease of the outermost PAH layer implies that the NH_3^+ pendant groups are compensated by the negative charges of PAA, and consequently, most of aliphatic groups in PAH chains are exposed at the surface, which would minimize the free energy of the system.

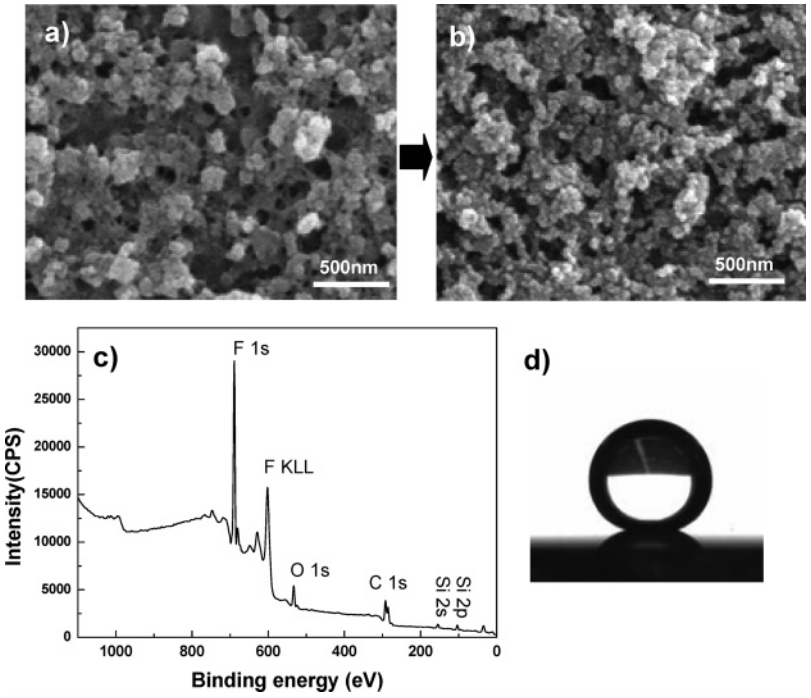

Figure 4. SEM images of (a) (PAH/PAA-coated $ZrO_2)_{10}$ film and (b) the film after deposition of silica nanoparticles. (c) XPS spectrum of the superhydrophobic organic−inorganic hybrid film after semifluorinated silane treatment. (d) Water droplet on this surface after fluorination.

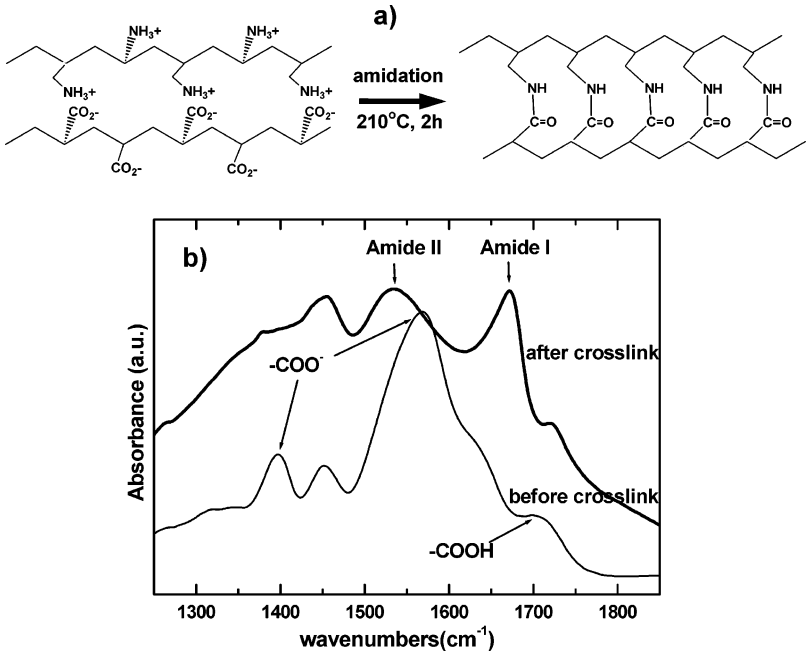

Figure 5. (a) Scheme of cross-linking reaction in (PAH/PAA-coated $ZrO_2)_n$ nanocomposite film. (b) FTIR-ERS spectra of (PAH/PAA-coated $ZrO_2)_{20}$ films before and after thermal cross-linking.

From our result, it was found that the wetting of solid surfaces can be controlled by the cyclic deposition of polyelectrolyte and charged nanoparticles. However, these surfaces have a high contact angle hysteresis, which is insufficient for the self-cleaning surface because of the hydrophilic character ($\theta < 90°$) of the PAH layer itself. To fabricate the artificial superhydrophobic surface, therefore, the porous (PAH/PAA-coated $ZrO_2)_n$ films were textured with 11 nm silica nanoparticles having hydroxyl groups, followed by fluorination by treatment with 1*H*,1*H*,2*H*,2*H*-perfluorodecyltrichlorosilane (FDS). Figure 4b shows the (PAH/PAA-coated $ZrO_2)_{10}$ bilayer film surface after deposition of silica nanoparticles, which results in the formation of a micro- and nanoscale binary structure similar to the lotus leaf, where every microscale papilla on the leaf surface is covered by nanoscale papillae. The water contact angles of (PAH/PAA-coated $ZrO_2)_n$ films deposited with silica nanoparticles are nearly zero exhibiting a superhydrophilic behavior, which means that the top surface of the film is covered with hydrophilic silica nanoparticles.

Prior to the perfluorosilane treatment, nanocomposite films were thermally cross-linked[42] at 210 °C for 2 h, because initially they were stabilized only by the electrostatic attraction between PAA and PAH. The amidation reaction of the nanocomposite film at 210 °C is reflected in the FTIR-ERS spectrum; specifically, heating causes the disappearance of the prominent peaks due to the $-COO^-$ and the appearance of amide peaks at ∼1540 and 1670 cm^{-1} (Figure 5). As seen in the IR spectrum,some protonated acid remains, but its absorbance peak

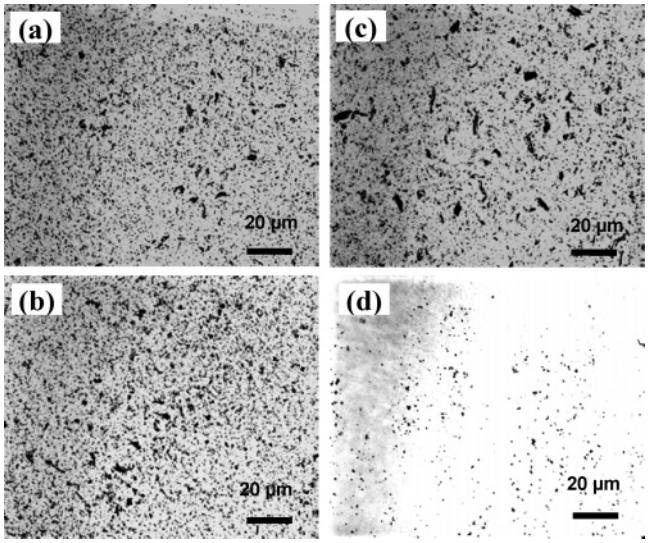

Figure 6. Photomicrography images of the film after heat-induced cross-linking (a), and of unheated hybrid films (c). (b) and (d) images show the etched morphologies of (a) and (c), respectively.

TABLE 1: Hardness Values of Various Nanocomposite Multilayer Films Determined by Nanoindentation

sample name	composition	hardness (GPa)	thickness (nm)
NH60	$(PAH/PAA)_{60}$, non-cross-linked	0.75	642.8
H60	$(PAH/PAA)_{60}$, cross-linked	1.36	576.0
ZH60	$(PAH/PAA\text{-coated } ZrO_2)_{60}$, cross-linked	2.15	712.9

shifts to higher wavenumbers, indicating a change in hydrogen bonding or environment. The existence of amide II bonds suggests more extensive cross-linking after heat treatment. This amidation enhances the chemical stability of the organic−inorganic nanocomposite film, as confirmed by the film's behavior upon being immersed in the ternary mixture H_2O/DMF/$ZnCl_2$ (3:5:2, w/w/w) for 30 min. Photomicrography images taken after etching the films in this ternary mixture (Figure 6) show that the residual fraction of covering for the heat-treated film (Figure 6b) is greater than that for the unheated film (Figure 6d). These results confirm that the heat-induced cross-linking greatly increases the chemical stability of these organic−inorganic nanocomposite films.

The surfaces were then fluorinated in FDS/hexane solution for 1 h. The fluorination of the nanocomposite surface was confirmed by X-ray photoelectron spectroscopy (XPS). The XPS spectrum in Figure 4c shows a strong fluorine peak at 688 eV. Figure 4d shows the shape of a water droplet on the surface of our nanocomposite films; the advancing water CAs were over 170° and the sliding angle was less than 2°, respectively. This result shows the Cassie state exhibiting a low contact angle hysteresis (receding contact angle only a few degrees less than the advancing contact angle). This lotus-leaf-like character remained after exposure of this surface to high humidity for more than 1 week.

Finally, the mechanical properties of our superhydrophobic organic−inorganic nanocomposite films were measured by nanoindentation. Hardness has been the most commonly studied property for organic−inorganic LBL multilayer films owing to the significant progress of the technique of nanoindentation.[45] Table 1 shows the average hardness values of various hybrid films. Sample NH60 was a pure polyelectrolyte film assembled over 60 deposition cycles from PAH and PAA solution. H60 with the structure of NH60 plus heat treatment had higher hardness compared with NH60. It is believed the hardness of $(PAH/PAA)_n$ polyelectrolyte multilayer film could be increased by heat-induced cross-linking. Furthermore, the incorporation of ZrO_2 nanoparticles into the polyelectrolyte film resulted in a notable increase in hardness values. In other words, the hardness of pure polymer multilayer films could be enhanced by the addition of an inorganic component (ZrO_2) and thermal cross-linking treatment (ZH60) even though these hybrid films have porous structures (Figure 2d). This finding shows a way to get significantly more functional materials.

Summary and Conclusions

We have presented a very simple electrostatic self-assembly fabrication of a stable organic−inorganic nanocomposite film having a superhydrophobic character. The proposed method is based on an LBL self-assembly process, in which the superhydrophobic surface can be easily developed by a simple procedure of about 10 deposition cycles of PAH and PAA-coated ZrO_2 nanoparticles and deposition of 1.5 bilayers of PAH and silica nanoparticles, followed by a simple fluorination. The proposed method could additionally be used as a simple method for fabricating PAH/PAA-coated ZrO_2 nanocomposite coatings with excellent chemical and mechanical durability for various applications.

Acknowledgment. This work was supported by a grant (Code No. 05K1501-01010) from the "Center for Nanostructured Materials Technology" under "21st Century Frontier R&D Programs" and the "National Research Laboratory Program" of the Ministry of Science and Technology, and BK21 program of Ministry of Education & Human Resources Development, Korea.

References and Notes

(1) Decher, G. *Science* **1997**, *277*, 1232.
(2) Wang, B. Q.; Rusling, J. F. *Anal. Chem.* **2003**, *75*, 4229.
(3) Park, J.; Hammond, P. T. *Adv. Mater.* **2004**, *16*, 520.
(4) Hiller, J.; Mendelsohn, J. D.; Rubner, M. F. *Nat. Mater.* **2002**, *1*, 59.
(5) Hiller, J.; Rubner, M. F. *Macromolecules* **2003**, *36*, 4078.
(6) Richert, L.; Lavalle, P.; Vautier, D.; Senger, B.; Stoltz, J.-F.; Schaaf, P.; Voegel, J.-C.; Picart, C. *Biomacromolecules* **2002**, *3*, 1170.
(7) Pastoriza-Santos, I.; Schöler, B.; Caruso, F. *Adv. Funct. Mater.* **2001**, *11*, 122.
(8) Shchukin, D. G.; Sukhorukov, G. B.; Möhwald, H. *Angew. Chem., Int. Ed.* **2003**, *42*, 4472.
(9) Rosidian, A.; Liu, Y.; Claus, R. *Adv. Mater.* **1998**, *10*, 1087.
(10) Xu, X. R.; Han, J. T.; Cho, K. *Chem. Commun.* **2003**, 966.
(11) Wenzel, R. N. *Ind. Eng. Chem.* **1936**, *28*, 988.
(12) Cassie, A. B. D.; Baxter, S. *Trans. Faraday Soc.* **1944**, *40*, 546.
(13) Barthlott, W.; Neinhuis, C. *Planta* **1997**, *202*, 1.
(14) Shibuichi, S.; Yamamoto, T.; Onda, T.; Tsujii, K. *J. Phys. Chem.* **1996**, *100*, 19512.
(15) Onda, T.; Shibuichi, S.; Satoh, N.; Tsujii, K. *Langmuir* **1996**, *12*, 2125.
(16) Xu, Y.; Fan, W. H.; Li, Z. H.; Wu, D.; Sun, Y. H. *Appl. Opt.* **2003**, *42*, 1.
(17) Lafuma, A.; Quéré, D. *Nat. Mater.* **2003**, *2*, 457.
(18) Nakajima, A.; Fujishima, A.; Hashimoto, K.; Watanabe, T. *Adv. Mater.* **1999**, *11*, 1365.
(19) Yoshimitsu, Z.; Nanajima, A.; Watanabe, T.; Hashimoto, K. *Langmuir* **2002**, *18*, 5818.
(20) Patankar, N. A. *Langmuir* **2003**, *19*, 1249.
(21) Soeno, T.; Inokuchi, K.; Shiratori, S. *Appl. Surf. Sci.* **2004**, *237*, 543.
(22) Zhang, X.; Shi, F.; Yu, X.; Liu, H.; Fu, Y.; Wang, Z.; Jiang, L.; Li, X. *J. Am. Chem. Soc.* **2004**, *126*, 3064.
(23) Jisr, R. M.; Rmaile, H. H.; Schlenoff, J. B. *Angew. Chem., Int. Ed.* **2005**, *44*, 782.
(24) Zhai, L.; Cebeci, F. Ç.; Cohen, R. E.; Rubner, M. F. *Nano Lett.* **2004**, *4*, 1349.
(25) Han, J. T.; Lee, D. H.; Ryu, C. Y.; Cho, K. *J. Am. Chem. Soc.* **2004**, *126*, 4796.
(26) Shirtcliffe, N. J.; McHale, G.; Newton, M. I.; Perry, C. C. *Langmuir* **2003**, *19*, 5626.

(27) Satoh, K.; Nakazumi, H. *J. Sol-Gel Sci. Technol.* **2003**, *27*, 327.
(28) Feng, L.; Song, Y.; Zhai, J.; Liu, B.; Xu, J.; Jiang, L.; Zhu, D. *Angew. Chem., Int. Ed.* **2003**, *42*, 800.
(29) Li, H.; Wang, X.; Song, Y.; Liu, Y.; Li, Q.; Jiang, L.; Zhu, D. *Angew. Chem., Int. Ed* **2001**, *40*, 1743.
(30) Feng, X.; Feng, L.; Jin, M.; Zhai, J.; Jiang, L.; Zhu, D. *J. Am. Chem. Soc.* **2004**, *126*, 62.
(31) Lau, K. K. S.; Bico, J.; Teo, K. B. K.; Chhowalla, M.; Amaratunga, G. A. J.; Milne, W. I.; McKinley, G. H.; Gleason, K. K. *Nano Lett.* **2003**, *3*, 1701.
(32) Xie, Q.; Xu, J.; Feng, L.; Jiang, L.; Tang, W.; Luo, X.; Han, C. C. *Adv. Mater.* **2004**, *16*, 302.
(33) Shirtcliffe, N. J.; McHale, G.; Newton, M. I.; Chabrol, G.; Perry, C. C. *Adv. Mater.* **2004**, *16*, 1929.
(34) Feng, L.; Zhang, Z.; Mai, Z.; Ma, Y.; Liu, B.; Jiang, L.; Zhu, D. *Angew. Chem., Int. Ed.* **2004**, *43*, 2012.
(35) Sun, T.; Wang, G.; Feng, L.; Liu, B.; Ma, Y.; Jiang, L.; Zhu, D. *Angew. Chem., Int. Ed.* **2004**, *43*, 357.
(36) Han, J. T.; Xu, X.; Cho, K. *Langmuir* **2005**, *21*, 6662.
(37) Han, J. T.; Jang, Y.; Lee, D.; Park, J. H.; Song, S.-H.; Ban, D.-Y.; Cho, K. *J. Mater. Chem.* **2005**, *15*, 3089.
(38) Erbil, H. Y.; Demirel, A. L.; Avci, Y.; Mert, O. *Science* **2003**, *299*, 1377.
(39) Li, M.; Zhai, J.; Liu, H.; Song, Y.; Jiang, L.; Zhu, D. *J. Phys. Chem. B* **2003**, *107*, 9954.
(40) Genzer, J.; Efimenko, K. *Science* **2000**, *290*, 2130.
(41) Nakajima, A.; Abe, K.; Hashimoto, K.; Watanabe, T. *Thin Solid Films* **2000**, *376*, 140.
(42) Harris, J. J.; DeRose, P. M.; Bruening, M. L. *J. Am. Chem. Soc.* **1999**, *121*, 1987.
(43) Pastoriza-Santos, I.; Caruso, F. *Adv. Funct. Mater.* **2001**, *11*, 122.
(44) Abdelsalam, M. E.; Bartlett, P. N.; Kelf, T.; Baumberg, J. *Langmuir* **2005**, *21*, 1753.
(45) Chan, C. M.; Cao, G. Z.; Fong, H.; Sarikaya, M.; Robinson, T.; Nelson, L. *J. Mater. Res.* **2000**, *15*, 148.